Performance of a Charring Ablator under Transient and Steady-State Convective and Radiative Heating

ROY M. WAKEFIELD* AND JOHN H. LUNDELL†
NASA Ames Research Center, Moffett Field, Calif.

Behavior of phenolic nylon under stepwise-varied heating conditions was investigated experimentally. Arbitrary transient heating pulses were generated by major variations in radiative heating and minor variations in enthalpy and pressure. Three rates of change of applied heating $\bar{r} = (\Delta\dot{q}/\Delta\tau)$ from 11 to 44 w/cm²-sec were provided by varying pulse times. Mass of material pyrolyzed m_p char interface recession X_c and surface recession X_s were determined over partial and complete pulses. The average degradation rates (m_p/τ or X_c/τ) increased with increasing $\bar{r}$, but the average surface recession rates (X_c/τ) were approximately the same for all pulses. The measured transient heating results were compared with material performance calculations based on steady-state heating test results. For minimum and maximum $\bar{r}$, respectively, measured degradation (m_p or X_c) was about 15% less and 30% more than calculated. The measured and calculated surface recession agreed within ±10% over all pulses. Although the quantitative results apply only to the phenolic nylon material and the transient test conditions of the present investigation, the effects are expected to be applicable to charring ablators under flight conditions. It is concluded that transients in material response in an increasing heating environment result in accelerated material degradation.

Nomenclature

h_t, h_w = stream and wall enthalpies, respectively, *Mj/kg*
m_p = pyrolysis mass loss per unit area, g/cm²; $\dot{m}_p = dm_p/dt$
p_s = test specimen surface pressure, atm
$\dot{q}_{app}$ = applied heating rate, w/cm²; $\dot{q}_{app} = \dot{q}c + \dot{q}r$
$\dot{q}_c$ = cold-wall convective heating rate, w/cm²
$\dot{q}_r$ = radiative heating rate, w/cm²
R_n = body nose radius, cm
$\bar{r}$ = mean rate of change of applied heating, w/cm²sec
t = time, sec
T_s = surface temperature, °K
X_c = char-interface recession, cm; $\dot{X}_c = d\dot{X}_c/dt$
X_s = surface recession, cm; $\dot{X}_s = dX_s/dt$
τ = total pulse time, sec

Introduction

AN ablating heat shield is exposed in flight to conditions that vary with time, but material evaluation tests in ground facilities are usually limited to steady-state heating conditions. There were two basic objectives in the present investigation: 1) to delineate and determine the significance of effects of transient heating on material behavior by generating and analyzing both transient and steady-state heating test data, and 2) to assess the applicability of results from steady-state heating tests to the analysis of material performance in a transient heating environment. Correlations of steady-state heating test results have been used, for example, in predictions of flight performance,[1] in the analysis of thermal protection systems in mission studies,[2] and for direct comparison with flight data.[3] A secondary objective in the present investigation was to develop experimental and analytical techniques for use in transient heating facilities such as the one described in Ref. 4. The heating conditions employed did not completely simulate atmospheric entry conditions but were obtained by major variations in the radiation heating rate with minor variations in the stream enthalpy and pressure. The ablation material examined was phenolic nylon.

Test Facility and Instrumentation

The Ames Entry Heating Simulator (Fig. 1)[5] comprises convective and radiative heating systems which can be operated either simultaneously or independently; the former is a wind tunnel with an electric arc-heated[6] supersonic stream, and the latter consists of a carbon-arc radiation source and two ellipsoidal mirrors. Radiation from the arc is collected by one mirror, reflected into a converging-diverging beam, and focused on the model by the other mirror. The beam passes through a quartz window in the downstream end of the test chamber. A shutter at the window controls the duration of the radiative heat flux. Wire-mesh screens are placed in the radiation beam to vary the heating level. A rotating chopper near the window periodically interrupts the incident radiation beam to eliminate reflected radiation during the measurement of test specimen surface temperature T_s.

The radiative and cold-wall convective heating rates ($\dot{q}_r$ and $\dot{q}_c$, respectively) and test specimen surface pressure (p_s) were measured with calorimeter and pressure probe models that had the same shape and were located in the same position as the ablation test specimens. To measure $\dot{q}_r$, the transient-type calorimeter[5] was blackened with camphor soot to produce a high surface absorptance. The pressure probe was made of copper and had a single $^1/_{16}$-in.-diam orifice leading from the stagnation point to tubing connected to a pressure transducer. The electrical signals from the calorimeter and pressure transducer were recorded on an oscillograph.

A monochromatic pyrometer was used to measure T_s in the brief interval during which the incident radiation was interrupted by the rotating chopper. The optical bandpass of the pyrometer was centered at ~0.84μ and was 0.2μ wide.

An automatic programing system was used to produce seven-step heating pulses composed of four steady-state heating conditions. The system provided changes in p_s, $\dot{q}_r$, and stream enthalpy h_t. To change stream conditions, the mass flow of air to the arc heater was varied while the power input was held constant. As the mass flow was increased

Presented as Paper 69-151 at the AIAA 7th Aerospace Sciences Meeting, New York, January 20–22, 1969; submitted March 7, 1969; revision received November 30, 1970.

* Research Scientist.
† Research Scientist. Member AIAA.

Table 1 Steady-state test conditions

Test condition	h_t, Mj/kg	$\dot{q}_c$, w/cm^2	$\dot{q}_r$, w/cm^2	p_s, atm
1	12.8	422	0	0.086
2	11.7	414	71	0.100
3	10.9	402	157	0.110
4	10.8	407	247	0.115

from minimum to maximum, h_t decreased 16% and p_s increased 33%. Consequently, $\dot{q}_c$ did not vary significantly over the operating range. The radiative heating input duration and levels, respectively, were controlled by actuating the shutter and by varying the number of screens placed in the radiation beam. For the initial and final steps, the shutter was closed and the test specimen was subjected only to convective heating. The intermediate steps were combined convective and radiative heating conditions ($q_{app} = \dot{q}_c + \dot{q}_r$), with the $\dot{q}_r$ level varied.

Description of Specimens and Tests

The test specimens, 1.9-cm-diam hemisphere-cylinders with a center core (Fig. 2a), were machined from phenolic-nylon, which had a density of 1.2 g/cm^3 and consisted of equal parts by weight of phenolic and nylon resins. Figure 2b is a photograph of the sectioned core of an ablated test-specimen. Surface recession (X_s) and char interface recession (X_c) depths are shown. The difference between the prerun core mass and the postrun core mass with the char removed is the pyrolysis mass loss m_p. It is the total amount of ablation products, char and pyrolysis gas, produced in degradation of the ablation material.[7]

At each of the four steady-state test conditions, $\dot{q}_c$, p_s, and $\dot{q}_r$ were determined in calibration runs (Table 1). The arc-heater plenum pressure and power input were monitored during all runs. The air stream enthalpy was calculated from the approximate relation[8]

$$h_t - h_w = K\dot{q}_c(R_n/p_s)^{1/2}$$

where K is 0.0088 (Mj/kg)(cm^2/w) (atm/cm)$^{1/2}$.

Conditions for the transient tests are illustrated in Fig. 3. Three different heating pulses were used, with nominal total times of 12, 24, and 48 sec. Each pulse consisted of seven steps (Table 2), and the test conditions in any given step were one of the sets of conditions given in Table 1. The applied heating rate ($\dot{q}_{app} = \dot{q}_c + \dot{q}_r$) was a minimum at the beginning of the pulse, increased to a maximum value at the midpoint, and decreased to a minimum again at the end. Because of the symmetry, the integrated applied heating is equal over the two halves of a pulse. The variations in p_s and $\dot{q}_r$ are similar to that for $\dot{q}_{app}$, whereas $\dot{q}_c$ is approximately constant, and h_t is slightly lower at the midpoint than at the beginning and end of the test pulse. Let us define a mean rate of change of applied heating, $\bar{r} = \pm\Delta q_{app}/\Delta\tau$, where Δq_{app} is the change in $\dot{q}_{app}$ from step 1 to 4 (or step 4 to 7) and $\Delta\tau$ is 44% of the pulse time. (This is the slope of the line indicated in Fig. 3.) Three values of $\bar{r}$ were obtained by varying τ as shown in Fig. 4, and Table 2. The τ's were selected to provide $\bar{r}$ values comparable to manned entry flights.

Table 2 Transient heating pulses

Pulse step	Test condition	Step duration, sec		
		Pulse L	Pulse I	Pulse S
1	1	6.6	3.4	1.7
2	2	5.9	3.0	1.4
3	3	6.2	3.0	1.6
4	4	11.4	5.8	2.8
5	3	6.5	3.1	1.5
6	2	6.1	3.1	1.5
7	1	5.9	2.8	2.0
Total time, sec		48.6	24.2	12.5
$\bar{r}$, w/cm^2-sec		11.0	21.9	44.2

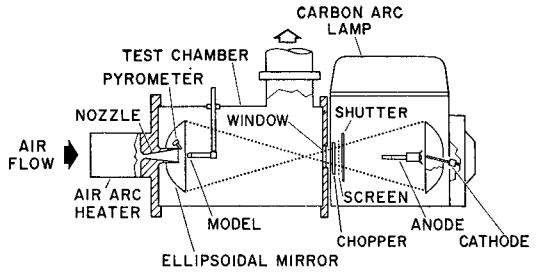

Fig. 1 Ames entry heating simulator.

Experimental Results

The transient heating tests were performed 1) over the complete pulses depicted in Fig. 4 and 2) over only the initial halves of these pulses, to investigate the integrated effects of increasing and decreasing $\dot{q}_{app}$. In pulse mode L, tests also were terminated at various times. The results are presented in Fig. 5. The absicissa is test time normalized by total time τ (which differed for L, I, and S). The data points are connected by lines for identification convenience—the lines do not imply uniform ablation rates for the time intervals between the test points. The values of m_p, X_s, and X_c and exposure time for each test specimen are also listed in Table 3.

In the steady-state heating tests, data were obtained at each of the conditions in Table 1. Figure 6 shows T_s and ablation measurements vs time for condition 1. Results for conditions 2-4 were similar, except that minimum test times were ~6 sec, and maximum test times ranged from 15 to 24 sec. After a transient period, the time variations of the ablation measurements became linear and T_s attained an essentially steady-state value. The slopes of the linear portions of these curves were used to determine $\dot{m}_p$, $\dot{X}_c$, and $\dot{X}_s$ (Table 4).

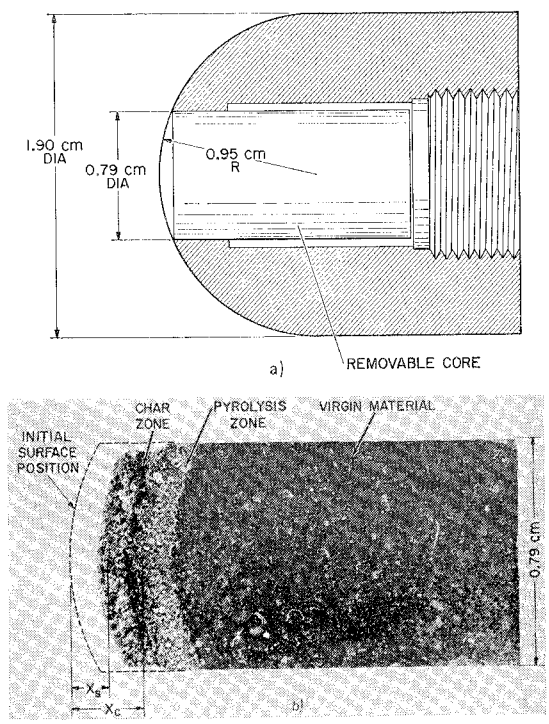

Fig. 2 Ablation test specimen.

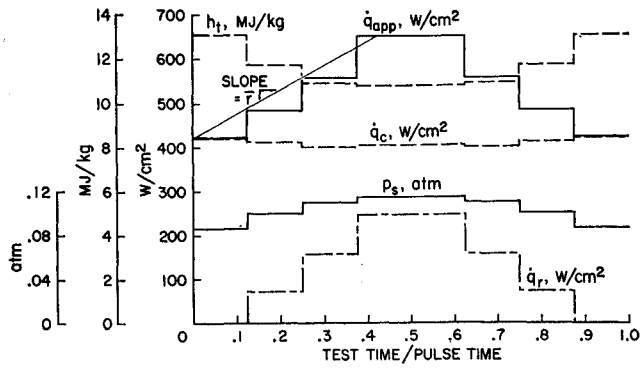

Fig. 3 Transient heating pulse conditions.

Discussion

The effects of the type of heating are seen by comparing Figs. 5 and 6. Under transient heating, m_p, X_c, and X_s have nonlinear variations with test time, in contrast to the linear results in steady-state heating. Also, T_s exhibits changes in rate of increase and level as the test conditions are varied in the transient case.

In addition, the integrated effects of transient heating can be demonstrated by comparisons of the test measurements for each half of a pulse. [Recall that, because of the symmetry, the integrated applied heating is the same for each half of a pulse (Fig. 3).] In all three cases, Δm_p and ΔX_c are greater under increasing heating (first half) than under decreasing heating (second half)‡; ΔX_s, however, is essentially the same for each half. Figure 7 shows that the average values of pyrolysis mass loss rate and interface recession rate increase 40% as $\bar{r}$ increases from 11 to 44 w/cm^2-sec, whereas the average surface recession rate is not strongly affected by $\bar{r}$ for the three pulse tests.

It is apparent that transients in the material response result from changes in the heating environment. Two types of transient response can be identified: the *initial ablation transient* that occurs at the beginning of ablation as the material develops a char layer and the *succeeding ablation transients* that occur with succeeding changes in test conditions.

The effects of initial heating on material response are shown by the steady-state heating data presented in Fig. 6. For $t < 6$ sec, the curves are nonlinear; the instantaneous values of $\dot{m}_p$ and $\dot{X}_c$ in this transient period are greater than the final steady-state values. Obviously, the test specimen in a transient heating test will also experience an initial ablation transient. The influence of this initial ablation transient on m_p and X_c is shown in Fig. 7. The significance of the effect is dependent on the duration of the initial transient relative to the total cycle time τ. That is, as τ is decreased, the effects of the initial ablation transient become more significant, and thus both m_p/τ and X_c/τ increase with $\bar{r}$.

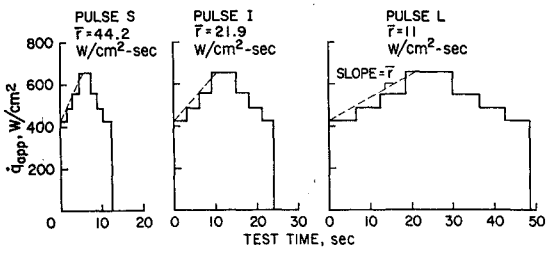

Fig. 4 Transient heating pulses.

‡ Material response over these periods is indicated, respectively, by the midpulse data points and by the increments between the ablation measurement for the complete pulse and midpulse data points (Fig. 5).

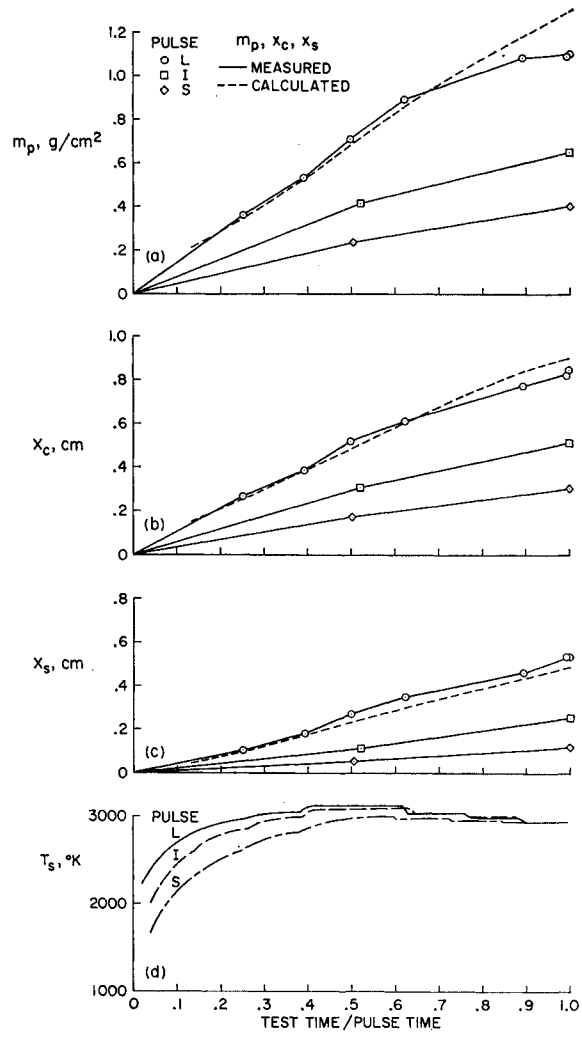

Fig. 5 Material response in transient heating.

The preceding results have indicated little effect of changes in the present test conditions on X_s. In the transient heating tests, ΔX_s was essentially the same for each half of a pulse, and X_s was not affected by $\bar{r}$. Mechanisms involved in surface recession of this material are complex and highly coupled. In general, surface recession is the result of both chemical reactions with the stream and pyrolysis gases and internal shrinkage which occurs as the material degrades.[9] The pyrolysis gases influence surface recession by inhibiting the diffusion of oxygen to the surface and by reacting in the gas phase with the stream oxygen. Thus, the production of pyrolysis gases may either suppress or increase the measured X_s. Unfortunately, there is not sufficient information in the present tests to separate these various mechanisms and effects.

Table 3 Transient heating test results

Pulse	τ, sec	m_p, g/cm²	X_s, cm	X_c, cm
L	12.2	0.361	0.11	0.27
	19.1	0.534	0.18	0.39
	24.2	0.711	0.27	0.52
	30.5	0.898	0.35	0.61
	43.4	1.087	0.46	0.77
	48.3	1.098	0.54	0.82
	48.6	1.106	0.54	0.85
I	12.6	0.413	0.11	0.31
	24.2	0.658	0.26	0.51
S	6.3	0.238	0.06	0.17
	12.5	0.407	0.12	0.31

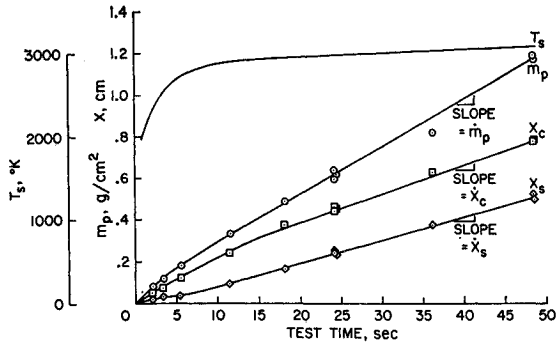

Fig. 6 Material response in steady-state heating at condition 1.

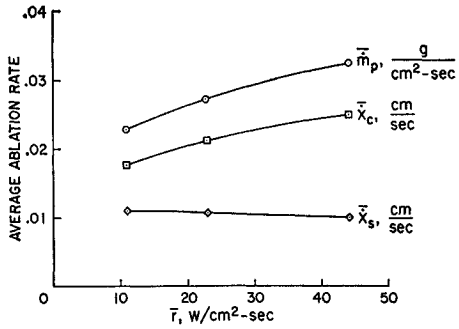

Fig. 7 Average ablation rates in transient heating.

Let us now consider effects of succeeding ablation transients. For pulse L, step 1 is nominally 6 sec long. As noted earlier, the initial ablation transient under steady-state heating at condition is also ~6 sec in duration. Therefore, the initial ablation transient has been completed at the beginning of step 2. Thus, to compare the effects of increasing and decreasing heating, let us consider $\Delta m_p/\Delta t$ over comparable segments of pulse L from steps 2–6. From step 2 to the midpoint of the pulse, $\Delta m_p/\Delta t \simeq 0.028$ g/cm²-sec, compared to ~0.020 g/cm²-sec from the pulse midpoint to the end of step 6. Such differences are attributed to the effects of the succeeding ablation transients. Let us examine those effects by comparing the measured transient heating results with calculated transient heating results that are based on the steady-state data but take into account the initial transient in the first step. Thus, any differences between the measured and calculated results will indicate the effects of the succeeding ablation transients.

For the calculations, m_p, X_c, and X_s for the first step were read from the nonlinear data fairings for condition 1 (Fig. 6). For the succeeding steps, the ablation rates from the steady-state heating tests were multiplied by the step duration to provide increments in m_p, X_c, and X_s. Finally, the increments were summed in succession for a complete transient heating pulse.

Calculated results for pulse L are represented in Fig. 5 bydashed lines, and it is apparent that inclusion of the initial ablation transient largely accounts for the transient ablation effects over the first half of the pulse. Over the latter part of this pulse, however, the measured values of m_p and X_c are less than the calculated values, whereas the measured X_s is greater than calculated.

Similar calculations performed for all three pulse tests are summarized in Fig. 8 as ratios of measured to calculated results vs normalized time. At the midpulse times the measured m_p exceeds the calculated value by 5, 13, and 28% for pulses L, I, and S, respectively. After the complete pulses, the measured values are 15% less, approximately equal to, and 19% greater than the calculated values, respectively. Note that during the first halves of the pulses, the m_p ratio exceeds one, indicating that an increase in $\dot{q}_{app}$ results in a period of accelerated degradation, similar to that occurring in the initial transient. The effects of the succeeding transients systematically decrease with $\bar{r}$. As $\bar{r}$ decreases, the time intervals at each condition in a pulse are lengthened, and the specimen may undergo periods of both transient ablation and constant-rate ablation of each test condition. In contrast, the m_p ratio decreases over the latter half of a pulse. Unfortunately, the data from the present program are not sufficient to determine the reason for this behavior.

Table 4 Steady-state heating test results

Test condition	$\dot{m}_p$, g/cm²-sec	$\dot{X}_s$, cm/sec	$\dot{X}_c$, cm/sec	T_s (final), °K
1	0.0229	0.0107	0.0140	3000
2	0.0229	0.0098	0.0180	3050
3	0.0265	0.0110	0.0189	3100
4	0.0301	0.0113	0.0201	3150

The X_c ratios in Fig. 8 display variations and trends similar to those observed in the m_p ratios. This is to be expected because m_p and X_c both indicate internal degradation response of the ablation material. Explanations for the transient effects on X_c are identical to those for m_p. The trends for X_s ratios are different. For pulse L, measured X_s's are 8–15% higher than calculated, and for pulses I and S, they are as much as 10% less than calculated. Thus, significant errors can result from use of steady-state heating test data to calculate material response in transient heating. Furthermore, the errors are dependent on the mean rate of change of applied heating.

Summary

The quantitative results of the present investigation apply only to the phenolic nylon material and the transient test conditions employed. However it is believed that the effects of transient heating on a charring ablator in flight and in the present investigation are qualitatively similar.

Transients in material response occur both during formation of a char layer and each time the heating conditions are changed. The transients occurring during increasing heating result in accelerated material degradation. The significance of the transient effects on material performance depends on the material response time relative to the test pulse time. As a

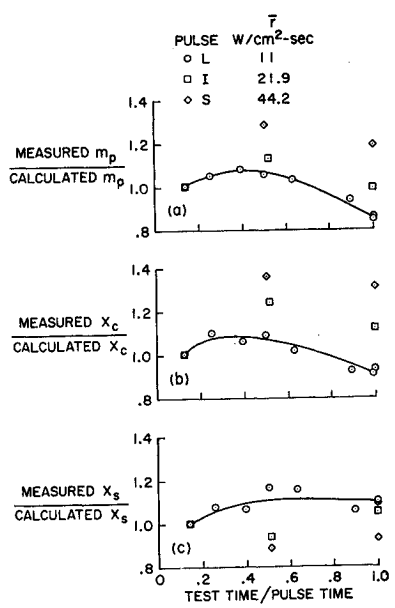

Fig. 8 Comparison of measured and calculated material response in transient heating.

result, average degradation rates over complete pulses increased with the mean rate of change of applied heating. Average measured surface recession rates were approximately constant, however.

The experimental transient heating ablation measurements were compared with calculated response based on steady-state heating test results. For minimum and maximum rates of change of applied heating, respectively, the measured degradation was ~15% less to 30% more than calculated over complete pulses, and 7% to 36% more than calculated during increasing heating. The corresponding measured surface recession measurements were approximately 10% more to 7% less than calculated over complete pulses, and 15% more to 10% less than calculated for increasing heating. These results indicate that the analytical procedures used in transient heating ablation cases should include analyses of the mechanism producing the transient effects.

References

[1] Strouhal, G., Curry, D. M., and Janney, J. M., "Thermal Protection System Performance of the Apollo Command Module," *AIAA/ASME 7th Structures and Materials Conference*, AIAA, New York, 1966, pp. 194–200.

[2] Brunner, M. J., Dolan, C., Grasier, R., Kottock, S., Merlo, G., "Study of Thermal Protection Requirements for a Lifting Body Entry Vehicle Suitable for Near-Earth Missions," Document No. 66SD253, May 12, 1966, General Electric Co., Philadelphia, Pa. (Final Report, NASA Contract NAS-2-2974).

[3] Hiester, N. K., Clark, C. F., and Vojvodich, N. S., "Ablative Characterization of Seven Heat Shield Materials—A Review of the NASA-SRI Round-Robin Program," *AIAA/ASME 10th Structures, Structural Dynamics and Materials Conference*, AIAA, New York, 1969, pp. 57–68.

[4] Gowen, F. E., and Nichols, F. H., "The Ames Combined Heating Facility," AIAA Paper 69-342, Cincinnati, Ohio, 1969.

[5] Lundell, J. H., Winovich, W., and Wakefield, R. M., "Simulation of Convective and Radiative Entry Heating," Symposium on Hypervelocity Technique, Denver, Colo., March 20–21, 1962.

[6] Shepard, C. E. and Winovich, W., "Electric-Arc Jets for Producing Gas Streams with Negligible Contamination," Paper 61-WA-247, American Society of Mechanical Engineers.

[7] Lundell, J. H., Wakefield, R. M., and Jones, J. W., "Experimental Investigation of a Charring Ablative Material Exposed to Combined Convective and Radiative Heating," *AIAA Journal*, Vol. 3, No. 11, Nov. 1965, pp. 2087–2095.

[8] Lundell, J. H., Dickey, R. R., and Jones, J. W., "Performance of Charring Ablative Materials in the Diffusion Controlled Combustion Regime," *AIAA Journal*, Vol. 6, No. 6, June, 1968, pp. 1118–1126.

[9] Wakefield, R. M., Lundell, J. H., and Dickey, R. R., "Effects of Pyrolysis-Gas Chemical Reactions on Surface Recession of Charring Ablators," *Journal of Spacecraft and Rockets*, Vol. 6, No. 2, Feb. 1969, pp. 122–128.

JUNE 1971 J. SPACECRAFT VOL. 8, NO. 6

Heating Environment and Protection during Jupiter Entry

MICHAEL E. TAUBER* AND ROY M. WAKEFIELD†
NASA Ames Research Center, Moffett Field, Calif.

The heating-rate histories and heat-shielding requirements for three different-sized Jupiter atmospheric probes, designed to survive entry, are studied parametrically. Atmospheres varying from 60% hydrogen-40% helium to pure hydrogen are considered. Recently, more sophisticated calculations of radiative absorption by ablation-product vapors have revealed large heating reductions at the body surface for steep Jovian entries. If up to half the probe's weight is devoted to heat protection, then steep, as well as shallow, angle entries appear feasible, assuming a graphite-class heat shield can function reliably at heating rates on the order of 100 kw/cm².

Nomenclature

A = base area of entry body, m²
C_D = drag coefficient
m = vehicle mass at any time t, kg
$\dot{m}$ = surface mass-loss rate per unit area, kg/m² sec
m_E = body mass at entry, kg
m_H = heat-shield mass; Δm_H ablated mass, kg
p_2 = shock-layer pressure, atm
$\dot{q}$ = heat-transfer rate, kw/cm²
$\dot{q}_R$ = radiative-heat-transfer rate; $\dot{q}_{R_{AD}}$ value for adiabatic shock layer
r_b = base radius of body, m
Re_{BT} = local Reynolds number for beginning of transition
t = time, sec
V_r = velocity with respect to rotating atmosphere, m/sec
γ_{IE} = inertial coordinate entry path angle, deg
Γ = radiative cooling parameter
δ_{AD} = adiabatic shock-layer thickness
θ_c = cone half-angle, deg
θ_s = cone shock-wave angle, deg
ρ = atmospheric density, kg/m³

Presented as Paper 70-1324 at the AIAA 7th Annual Meeting and Technical Display, Houston, Texas, October 19–22, 1970; submitted October 19, 1970; revision received March 1, 1971.

* Research Scientist, Hypersonic Free-Flight Branch, Vehicle Environment Division. Associate Fellow AIAA.

† Research Scientist, Thermal Protection Branch, Thermo- and Gas-Dynamics Division.

Introduction

THE velocity of entry into the Jovian atmosphere will exceed 60 km/sec. A previous paper[1] showed that heat-shield ablation might be kept within tolerable limits by making near equatorial posigrade entries (i.e. in the direction of planetary rotation) at very shallow flight-path angles, holding Reynolds numbers below selected values to avoid transition to turbulent flow (assumed to be intolerable). Four atmospheric compositions ranging from pure hydrogen to pure helium were considered, and combinations of bodies and trajectories which could succeed for all atmospheric compositions were found. The design in such a case, where atmospheric composition is unknown, must be a compromise of the optimum designs for each specific atmosphere. In